Regeneration of the neurogliovascular unit visualized in vivo by transcranial live-cell imaging

Margarita Arango-Lievano, Yann Dromard, Pierre Fontanaud, Chrystel Lafont, Patrice Mollard, Freddy Jeanneteau

Regeneration of the neurogliovascular unit visualized *in vivo* by transcranial live-cell imaging

Margarita Arango-Lievano [1*], Yann Dromard[1*], Pierre Fontanaud [1,2*], Chrystel Lafont [1,2], Patrice Mollard [1,2], Freddy Jeanneteau [1]

[1]Institut de Génomique Fonctionnelle, University of Montpellier, CNRS, INSERM, 34094 Montpellier, France

[2]BioCampus Montpellier, University of Montpellier, CNRS, INSERM, 34094 Montpellier, France

[*] Co-first authors by alphabetical order

freddy.jeanneteau@igf.cnrs.fr

Keywords

Transcranial 2-P microscopy, transcranial epifluorescence microscopy, functional angiography, pericytes, astrocytes, neurons, CNS diseases

Abstract

Functional imaging in behaving animals is essential to explore brain functions. Real-time optical imaging of brain functions is limited by light scattering, skull distortion, timing resolution and subcellular precision that altogether, make challenging the rapid acquisition of uncorrupted functional data of cells integrated *de novo* in the neurogliovascular unit. We report multimodal transcranial *in vivo* optical imaging for the fast and direct visualization of microcirculation in the perfusion domain where new cells incorporated in the neurogliovascular unit during the progression of a seizure disorder and its treatment. Using this methodology, we explored the performance improvement of cells integrated *de novo* in the neurogliovascular unit. We report fast transcranial imaging of blood microcirculation at sites of pericyte turnover in the epileptic brain and after treatment with a trophic factor that revealed key features of the regenerating neurogliovascular unit.

Introduction

The neurogliovascular unit is a complex assembly of endothelial cells, perivascular mural cells, extracellular matrix, astrocytes and neurons (Stanimirovic and Friedman, 2012). Each interface between the various cell types assembled in the neurogliovascular unit serves particular functions by way of paracrine signaling with specific receptor systems (Abbott et al., 2006; Sweeney et al., 2019). Mural cells are embedded in the basal membrane of the blood brain barrier (BBB) and the vessel walls connecting with neuronal axons, astrocytes and endothelial cells where it regulates the exchange of nutrients, metabolites and solute between blood and interstitial milieu in the brain, and ensures local energetic supply with spatial and temporal precision (Grutzendler and Nedergaard, 2019; Harris et al., 2012; Iliff et al., 2014). Sensory stimulation, neuronal activity and learning new experience command to the mural cells with a vascular response suited to the local activity of the neuronal network (Hill et al., 2015; Kisler et al., 2020; Whiteus et al., 2014). Mural cells specialize into pericytes and smooth muscle cells (SMC) that cover more than 90% of the cerebrovasculature (Armulik et al., 2011; Trost et al., 2016; Zhao et al., 2015).

Imaging studies of the living mouse brain over months in adulthood indicated that both the mural cells and microvessels establish very stable interface of contacts (Arango-Lievano et al., 2018; Berthiaume et al., 2018) that contrasts with its extensive dynamic sprouting and pruning during development (Armulik et al., 2010; Coelho-Santos and Shih, 2020; Daneman et al., 2010; Gaengel et al., 2009). However, dynamic remodeling of perivascular mural cells has been reported in the ageing human brain (Montagne et al., 2015) as well as in various vascular pathologies of the adult central nervous system (Sweeney et al., 2019). Neurological diseases associated with pericytosis include Alzheimer's disease (Sagare et al., 2013), cerebral amyloid angiopathy (Giannoni et al., 2016), stroke (Fernandez-Klett et al., 2013), vascular dementia (Iadecola, 2013), cerebral autosomal dominant arteriopathy with subcortical infarcts leukoencephalopathy (Ghosh et al., 2015), epilepsy (Leal-Campanario et al., 2017), Amytrophic lateral sclerosis (Winkler et al., 2013), traumatic brain injury (Zehendner et al., 2015), neonatal intraventricular hemorrhage (Braun et al., 2007) and others presented in excellent reviews (Lendahl et al., 2019; Rasmussen et al., 2018; Sweeney et al., 2019; Zlokovic, 2008).

Although we know a lot about the individual functions of vessels, pericytes, astrocytes and neurons in the healthy and diseased brains, little is known about their roles as a network organizing the neurogliovascular unit (Iadecola, 2017). Would the damage of one cell type

disorganize the structure and function of the neurogliovascular unit? The sole optical ablation of a small number of pericytes in the healthy brain suggested that the neurovasculature tolerates fluctuations of pericytes coverage without damaging consequences in the healthy brain. In fact, pericytes use PDGF-BB and ephrin signaling to regain coverage within days by the extension in non-overlapping territories of neighboring pericytes for bridging the gaps in vascular coverage (Armulik et al., 2010; Berthiaume et al., 2018; Foo et al., 2006; Salvucci et al., 2009). This scenario reads different in the context of CNS diseases as pericytosis, induced either constitutively or conditionally, resulted in neuroinflammatory microbleeds (Ogura et al., 2017; Park et al., 2017; Rustenhoven et al., 2017), circulatory failure and tissue anoxia that precede neurodegeneration and cognitive impairment (Bell et al., 2010; Kisler et al., 2017; Kisler et al., 2020; Montagne et al., 2018; Nikolakopoulou et al., 2019). Therefore, pericytosis accelerates CNS diseases progression by degrading barrier and perfusion functions of the neurogliovascular unit (Winkler et al., 2011).

This raises important questions about the repair of the neurogliovascular unit. How would new cells integrate structurally in the topological organization of the damaged neurogliovascular network? Would the new cells be operating isolated or integrated into the damaged neurogliovascular network? Wouldn't new cells operate as the network, damaged or healthy, depending on the physiological microenvironment and disease state of progression? Would changing the local ratio between individual cell types organizing the neurogliovascular unit modify its function? There are limitations that make answering these questions challenging. First, it requires a longitudinal approach to track the regeneration of the damaged neurogliovascular unit. Second, it requires an *in vivo* approach to investigate the complex multicellular organization and topology of the neurogliovascular unit in its physiological environment. Third, it requires a non-invasive approach to visualize the newly formed cells and its dynamic assembly in the damaged neurogliovascular unit. Fourth, it requires non-invasive techniques for tracking endophenotypic parameters of disease progression and performance improvement of the neurogliovascular unit in its naturalistic surrounding tissue. Fifth, it requires a treatment that would promote the regeneration of the neurogliovascular unit. In this regard, trophic factors and guidance molecules show promising prospects for the clinic because they promote the assembly, growth and survival of cells organizing the neurogliovascular unit (Maki et al., 2013; Xing and Lo, 2017). Studies that used PDGF-BB as treatment of vascular pathology in models of stroke

(Shibahara et al., 2020) and epilepsy (Arango-Lievano et al., 2018) reported regrowth of perivascular mural cells with amelioration of the neuropathology and behavior.

We present a methodology to visualize the regeneration of the neurogliovascular unit with cellular precision and test performance improvement in the physiological environment of the disease state of progression. We report fast transcranial imaging of blood microcirculation at sites of pericyte turnover in the epileptic brain and after treatment with a trophic factor that revealed key features of the regenerating neurogliovascular unit.

Methods and Materials

Animal model and experimental timeline

It requires a time-lapse approach to capture the acts of regeneration of the neurogliovascular unit and to test its performance improvements. We planned a longitudinal experiment for tracking vasoactive phenomena in its physiological environment with high-speed microscopy. The timeline is divided in 3 imaging sessions in the same animal subjects overtime to assess: 1) homeostasis, 2) damages due to disease onset and 3) functional improvement with treatment compared to placebo. The objective is to track how the newly formed cells integrate functionally in the neurogliovascular unit in its physiological environment. To this end, we used transcranial optical imaging techniques for tracking endophenotypic parameters of disease progression in its naturalistic surrounding tissue (Figure 1). Given that only a small field of view can be repeatedly imaged safely, the animal subjects were sacrificed on completion, for brain-wide clinical inspection of neurogliovascular markers. Such procedure will aid determining if cells newly integrated in the neurogliovascular unit operate equally in the healthy and sick brains.

We chose to investigate the regeneration of the neurogliovascular unit in a mouse model of epilepsy (Ben-Ari, 2012). Fifty percent of mice injected i.p. with kainic acid (25 mg/kg, Sigma-Aldrich) developed within 3 hours at least one status epilepticus associated with the generalization of seizures with widespread anatomical repercussions in the brain including the sensory cortex that was imaged. To administer the intraveinous treatment (saline only or with 100 µg PDGF-BB in a volume of 50 µl once a week for 3 weeks, Sigma Aldrich), mice were lightly sedated with isoflurane and a drop of ophthalmic anesthetic before retro-orbital sinus injection.

All procedures followed the Directive by the Council of the European Communities (86/609/EEC) and were reviewed and approved by the institutional animal care and use

committee at the University of Montpellier and the French ministry of research (protocols 00846.01 and 00651.01). All efforts were made to minimize the number of animals used and their suffering. Animals were housed under a 12 hr light/ dark cycle with unrestricted access to food and water. Male animals were used at 4 months of age at the beginning of the procedure.

Direct visualization of the neurogliovascular unit in its physiological environment is necessary to track the remodeling of its multicellular organization (Figure 2A). Although, autofluorescence 2-photon microcopy can distinguish between the venogram and arteriogram in absence of contrasting agents (Li et al., 2020), its low resolution prompted us to use fluorescent tracers for *in vivo* optical imaging due to its subcellular resolution and limited toxicity. Diffusible and tethering chemical dyes or protein dyes can be used for imaging of vessel specifications with hydrazide-AlexA633 (1 mg/kg injected 24h prior, ThermoFisher Scientific) (Shen et al., 2012), for imaging the vascular bed with small and large molecular weight dextrans (50-150 mg/kg from Applied Biosystems and Sigma Aldrich) (Lafont et al., 2010), for imaging the vasculature with lectins (0.1 mg/ml from *Lycopersicon esculentum,* Sigma-Aldrich) (Di Giovanna et al., 2018), for imaging the pericytes on capillaries and post-capillary venules with the Neurotrace (1 µg injected days prior, ThermoFisher Scientific) (Damisah et al., 2017), for imaging the astrocytes bound to vessels with sulforhodamine SR101 (20 mg/kg from ThermoFisher Scientific) (Hill and Grutzendler, 2014; Hulsmann et al., 2017), and to visualize tissue oxygenation with pimonidazole (Sigma Aldrich) (Whiteus et al., 2014). Specific antigens expressed by the astrocytes, neurons, mural cells or endothelial cells are instrumental for genetic tracing with fluorescence indicators and visualizing their functional interfaces in real-time *in vivo*.

Here, we used the membrane-bound tdTomato to mark the mural cells with subcellular precision by crossing the line Tg(Cspg4-cre)1Akik/J (Jackson labs stock 008533) with Ai27(RCL-hChR2(H134R)/tdT)-D (Jackson labs stock 012567) (Arango-Lievano et al., 2018), and also with the line Tg(Thy1-YFP)HJrs/J (Jackson labs stock 003709) to label pyramidal neurons with synaptic precision (Arango-Lievano et al., 2019). Vessel categories are easily recognized by pericyte morphologies (Figure 2B) and by the direction of flow. This was useful for tracking performance improvements of each cell types *in vivo* between imaging sessions. All data collected in animals were from littermate controls.

Transcranial 2-photon microscopy

Mice were anesthetized with a mix of 0.075mg/g ketamine and 0.01mg/g xylazine and lidocaine sprayed atop the skull prior to surgery. Thin-skull preparation for transcranial *in vivo* imaging was performed as previously described (Arango-Lievano et al., 2016). Skull bone was thinned between imaging sessions down to 18-20 μm thick using disposable ophtalmic surgical blades (Surgistar). The scalp is sutured and topped with antibiotic cream to avoid infection between imaging sessions. A detailed map of the pial vasculature was taken at macroscopic and microscopic scales for subsequent relocation. Three sessions were performed to compared basal state with the effects of seizures and treatment.

All images were acquired with a Zeiss LSM710 2-photon microscope coupled to a Ti:sapphire laser (Chameleon vision2, Coherent) and a water immersion 20x objective (NA 1.0, Apochromat, Carl Zeiss) for optimal fluorophore excitation and emission separation. Excitation wavelengths avoided 2-photon excitation wavelengths (880-920 nm) for ChR2 stimulation (Andrasfalvy et al., 2010) but were optimal for tdTomato and dextran-FITC excitation (1040 nm and 780 nm, respectively). ChR2-tdTomato could not be activated at these excitation wavelengths (Andrasfalvy et al., 2010). Laser power kept below 5 mW is not compatible with ChR2 stimulation but necessary for non-damaging longitudinal studies. Images were taken at each image session for each mouse using 0.75 μm step with a scanning dwell time of 2.55 μsec per pixel. Image subfields were stitched together using ImageJ stitching plugin. All images obtained from time lapses imaging sessions were realigned with Image J plugin RegStack to minimize artifacts of heartbeat pulsations and blood pressure. The volume of the field of view (volume 500 x 500 x 250 μm) was reconstructed with Imaris 8.0 (Bitplane) from z-stack images (512 x 512 pixels). Mural cells skeleton were traced using the filaments tracer module of Imaris, which calculated the surface of vessels covered by mural cells. Sets of coordinates of the 3 different imaging sessions were extracted with the Edlund method in order to align the coordinates with a stable reference point and further point-by-point analysis using MatLab (Mathworks). Mural cells extensions and retractions on vessel walls were measured by subtraction of signal between consecutive images.

Transcranial epifluorescence time-lapse microscopy

Mice were anesthetized with a mix of 0.05mg/g ketamine and 0.01mg/g xylazine and lidocaine sprayed atop the skull prior to thinning. Relocation of the field of view previously imaged with

the 2-photon microscope was made possible with both macroscopic and microscopic objectives and tunable magnification of the stereomicroscope (from 8x to 600x). Zones of interest corresponded to sites where vessel coverage with *NG2-tdTomato* mural cells changed between imaging sessions as determined by prior 2-photon microscopy. Two sessions were performed to assess the effect of seizures and treatment. Transcranial blood flow was imaged through a thinned skull preparation with an epifluorescence Discovery V12 microscope (Carl Zeiss) equipped with a 20x, 63x water objectives (Carl Zeiss). To measure velocities of red blood cells (RBCs) in individual vessels, retro-orbital injections of a solution of 70-kDa Dextran-Texas red (Sigma-Aldrich) were performed to fluorescently label the plasma but not red cells permitting identification of their circulation. Fluorescence excitation was delivered by a Lambda LS xenon arc lamp (300W; Sutter Instruments) fitted with a fast-rotating filter wheel (27 milliseconds lag) and linked to the stereomicroscope with an optical fiber. Fluorescence emission was captured with a sCmos camera (C11440 Orca-Flash 4.0, Hamamatsu Photonics) capturing images at 100 to 800 Hz. To allow accurate quantification of flow velocities in vessels with widely varying diameters (between 5 to 100 µm) such as brain microvasculature, several movies were acquired with MetaMorph software (Molecular Devices) in the same field at different focus and different magnifications and resolution (512 x 512 pixels). With the 20x objective, the speed limit was up to 5 mm/s if images were taken at 100 Hz, 9 mm/s at 200 Hz, 14 mm/s at 400 Hz and up to 17 mm/s at 800 Hz.

RBC flow was analyzed from 10,000 images per field using an in-house Matlab sofware based on an algorithm as described (Kim et al., 2012). Matlab code for LS-PIV (Line-Scanning Particle Image Velocimetry) available at: https://sourceforge.net/projects/lspivsupplement/files). Briefly, one line was traced along the center lumen of the vessel. Parallel line-scans were automatically traced from the reference line and the emission fluorescence along this ribbon along the vessel was averaged and instantaneous red blood cell flow was measured. Two Fast Fourier Transform (FFT) were sequentially applied, a cross-correlation on the spatial frequency domain was performed, and inverse FFT on cross-correlation gave access to a correlation peak. Peak shift from the origin obtained by fitting a Gaussian function gave a peak distance shift value in pixels/frames converted as mm/sec according to image acquisition parameters. These analysis sequences were applied to multiple regions of interest. We used factorial ANOVA (Prism 8.0

GraphPad) to compare multiple groups, using seizures, PDGF-BB, and vessel subtypes as independent factors, followed by post-hoc comparison with Sidak test.

Open skull cerebrovascular angiography

Mice were anesthetized with a mix of 0.075mg/g ketamine and 0.01mg/g xylazine and lidocaine sprayed atop the thinned skull window prior to surgery. A 3–4 mm craniotomy was prepared over the somatosensory cortex and the underlying dura was removed. This is a terminal session for *in vivo* imaging at the open skull preparation that facilitates access of drugs via the surface of parietal cortex. Baseline vessels dynamics were captured in HEPES-buffered ACSF (in mM 120 NaCl, 3.5 KCl, 0.4 KH2PO4, 15 glucose, 1.2 CaCl2, 5 NaHCO3, 1.2 Na2SO4, 20 HEPES, pH = 7.4) for 5 min prior addition of 10^{-4} M glutamate (Sigma Aldrich) for 15 min, 10^{-8} M endothelin-1 (Sigma Aldrich) for 15 min. Dextran dyes 10-Kda and 70-Kda were injected i.v. to mark vessels and track its permeability. After 2 h of Dextrans injection, the remaining circulating tracers were rinsed out of the circulation with PBS by transcardiac perfusion. The fluorescent tracers observed in cells and in the brain parenchyma of post-mortem tissues can only result from diffusion through the vessel walls normally non-permeable to these dyes. Indeed, no parenchymal dextran was observed in healthy control mice that were not subjected kainate-induced seizures.

Movie correction from movement due to respiration and blood pressure were done using the ImageJ plugin Image stabilizer. Vessel diameters were calculated at cross sections using imageJ plugin plot profile, visualization of vessel diameter elasticity over time was obtained using the dynamic reslice plugin. We used factorial ANOVA (Prism 8.0 GraphPad) to compare multiple groups, using seizures, PDGF-BB, and vessel subtypes as independent factors, followed by post-hoc comparison with Sidak test. Significance level is set at α=0.05.

Results

Multimodal transcranial optical imaging as diagnostic mode

Implementation of *in vivo* transcranial epifluorescence imaging of hemodynamics combined with 2-photon cellular imaging and functional angiography for longitudinal tracking of neurogliovascular plasticity allowed degenerative and regenerative changes in the neurogliovascular unit to be monitored during disease progression and upon treatment (Figure 3).

Focal plan images were taken every 0.75 μm step within a depth of 250 μm for a total volume of 3.6 mm^3 for capturing the topological organization of the cerebrovasculature at each session.

Comparing the first 2 sessions of transcranial 2-photon imaging indicated that seizures caused the retraction of a transition pericyte from its underlying arteriole a1 at about 75 μm under the surface of the brain. Cellular debris visible in the field of view of the second image is suggestive of pericytosis associated with a dilation of the underlying vessel (Figure 3A). High-speed imaging of RBC velocity using transcranial *in vivo* epifluorescence miscroscopy allowed visualizing a rare backflow event in the arteriole a1 where the transition pericyte retracted after seizures (supplemental movie 1). This impacted flow velocities calculated in neighboring vessels. That is, acceleration in the arteriole branch a2, mixed effects in capillaries and acceleration in the venule V (Figure 3B).

Comparing the 2nd (after seizure induction) and 3rd (after treatment) 2-photon images in the same field of view allowed direct visualization of pericyte extension at a similar position on the arteriole a1 suggestive of pericyte regeneration that associated with the normalization of the underlying vessel diameter (Figure 3A). A second transcranial *in vivo* epifluorescence imaging session of the same field of view indicated that blood flow normalized in all vessels (Figure 3B and Supplemental movie 2). This result is direct visual evidence that pericyte extension in the context of seizure treatment with PDGF-BB ameliorated RBC velocity in the underlying arteriole and in the surrounding vascular bed.

To interrogate the structural impact of pericyte remodeling on local vasodynamics, we used time-lapse 2-photon *in vivo* microscopy of vessels in response to vasoactive drugs applied topically through a cranial window. Glutamate is an established vasodilator of capillaries (Hall et al., 2014) and endothelin-1 a known vasoconstrictor (Dehouck et al., 1997) through its receptor EDNA enriched in the smooth muscle cells (SMC) (He et al., 2016; Kumar et al., 2017). We relocated the same field of view to capture the dynamics of vascular plasticity at the sites of pericyte regeneration on arteriole a1 and its neighboring vessels (supplemental movies 3 and 4). Time-lapse analysis showed that the pericyte newly formed on arteriole a1 responded poorly to glutamate and robustly to endothelin-1 compared to the nearest pericyte on arteriole a2 (Figure 3C). Such a methodology allowed direct visualization of local vasoactivity associated with pericyte degeneration and regeneration events.

Quantitative analysis of vasoactivity where pericytes degenerated and regenerated

We conducted an extensive analysis of the structure and function of the newly formed pericytes to assess its performance on the neurogliovascular unit compared to the pre-existing pericytes. We segmented the cortical vascular bed to provide a size- and type-specific analysis of mural cells on a topological basis. Glutamate evoked the dilation of capillaries and the contraction of pre-capillary arterioles with a slight delay (Figure 4A), which could safely optimize blood circulation in the surrounding perfusion domain as previously suggested (Iadecola et al., 1997). This effect was more robust at vessels covered with mural cells than vessels lacking mural cells (Figure 4B). Likewise, the effect of endothelin-1 lasted longer if arterioles were covered with SMC rather than not covered with SMC (Figure 4B).

Overall, the newly formed pericytes on capillaries and venules did not distinguish from the pre-existing pericytes in terms of attributes to these vasomodulatory drugs. We found no difference if vessels were always covered with pericytes or gained coverage with treatment (Figure 4C). Likewise, there was no difference if vessels were never covered with pericytes or lost coverage after seizure induction (Figure 4C). It means that adding a pericyte predicts capillary dilation to glutamate whereas loosing a pericyte predicts no response. In contrast, the SMC newly formed after seizures or treatment showed mixed responses to glutamate compared to the pre-existing SMC in the healthy controls. It is not merely a lack of contractility of the newly formed SMC since they responded to endothelin-1 (Figure 4C).

Statistical analyses of group data (Figure 4D) indicated that adding a new SMC or loosing a pre-existing SMC is not merely similar to vessels always covered with SMC ($P<0.0001$) or never covered with SMC ($P=0.02$). Treatment of seizures showed statistical difference between PDGF-BB and placebo in the analysis of vasoactivity of the arterioles ($P=0.035$ for the newly formed SMC) and the capillaries ($P=0.03$ for the newly formed pericytes). This could be due to the trophic effects of PDGF-BB that offset seizure-induced pericytosis by increasing the number of SMC and pericytes (Arango-Lievano et al., 2018).

Pericyte turnover alters local blood perfusion

By imaging at a rate of 0.8 kHz, we could observe the heartbeat's influence on flow at about 160 pulses.min^{-1}, which is in synchrony with arterial pulsations as previously described (Mateo et al., 2017). The average flow was calculated as the mean of RBC velocities in epochs of at least 2

seconds (Figure 5A). As cerebrovascular RBC velocities can markedly change from a vessel to another (up to 20x), we imaged short episodes (2 to 30 seconds) at varying acquisition rates (100-800 frame per second). Imaging bouts were spaced ~2 min apart to prevent photobleaching, photodamage and tissue heating. We found that the speed of flow is proportionate to vessel diameter in the range of 7-40 µm for both the arterioles and venules (Figure 5B). In the capillaries (< 7 µm), the flow is not proportionate to the vessel size.

To determine the performance of the newly formed pericytes at moderating blood flow, we compared vessels that gained or lost a pericyte with vessels that were covered or not covered with pre-existing pericytes. We found that after seizures, blood flow at the sites of pericyte gains and losses was not proportionate to vessel size. This contrasted with the speed of flow at the sites of pericyte turnover after treatment of seizures with PDBG-BB (Figure 5C). The performance of the newly formed pericytes after treatment with PDGF-BB fits with the moderating effects of the pre-existing pericytes in healthy controls.

Statistical analyses of group data (Figure 4D) indicated that loosing a pre-existing pericyte (P=0.003) or a pre-existing SMC (P=0.0007) is not merely similar to the absence of pericytes or SMC for moderating the flow. This contrasted with the newly formed pericytes or newly formed SMC that operated similarly to the pre-existing ones regardless of seizure treatments. Overall, the turnover of mural cells moderates the perfusion domain by increasing flow in the capillary bed after seizures due to a net loss of pericytes and the occlusion of underlying vessels (Figure 4D). On the contrary, the trophic effects of PDGF-BB are consistent with the moderation of flow in the perfusion domain by increasing the number of new pericytes and SMC according to the topology of the neovasculature.

Pericyte turnover at vessel bifurcations impacts the perfusion domain

Pericyte's cell bodies often reside at vessel bifurcations extending coverage across multiple branches in the capillary bed (Figure 2B). We wondered whether such an anatomical position is suited to direct circulation in specific perfusion domains. To address this possibility, we tracked *in vivo* vessel perfusion at sites of mural cells retractions and extensions across vessel branches after treatment of seizures (Figure 5E). SMC extension precisely at an arteriole bifurcation associated with changes of blood flow between vessel branches (see arrows). Pericyte retraction

associated with the occlusion of the underlying capillary, diverting flow in the bifurcation to the vessel branches where pericyte extended coverage (see arrows).

Pericyte turnover at vessel bifurcations impacts its permeability

Post-mortem analysis of the angiogram performed prior sacrifice with the small 10-Kda dextran dye showed its prominent extravasation at vessel bifurcations in venules (Figure 6A), in arterioles (Figure 6B) and in the capillary bed (Figure 6C). Endothelial cells and pericytes loaded with the dye at vessel bifurcations whereas astrocytic endfeet and neurons loaded with the dye beyond bifurcations, suggesting its diffusion along the basal membrane and in the parenchyma.

Consistent with the extravasation of the dye, the co-labeling of *NG2-tdTomato* pericytes with a marker of cell death was observed at a vessel bifurcation (Figure 6D). Likewise, the co-labeling of *NG2-tdTomato* pericytes with a marker of cell proliferation was observed at a vessel bifurcation (Figure 6E). Such post-mortem evidence combined with the time-lapse visualization of *NG2-tdTomato* debris clearance between imaging sessions indicate that mural cells extensions and retractions are not the result of cell migration in and out of the field of view but rather associated with pericyte degeneration and regeneration events.

Discussion

Multimodal optical transcranial imaging techniques were combined in a longitudinal protocol to assess the performance of cells newly integrated in the neuroglovascular unit during the progression of a seizure disorder and its treatment. We found that pericyte regeneration assumed functional attributes similar to those of the pre-existing pericytes in moderating blood flow. Pericyte turnover occurred at vessel bifurcations to optimize its effects on the surrounding perfusion domain. This methodology can be used as a diagnostic mode to monitor performance improvement of tissue regeneration in its physiological environment. It adds to prior studies that used invasive *in vivo* imaging to show that both the vascular and axonal networks can recover after traumatic injury (Fenrich et al., 2012; Tedeschi et al., 2016).

Keeping the skull is important for accurate measures of vascular dynamic signals as craniotomy is known to cause inflammation (Cole et al., 2011; Lagraoui et al., 2012; Xu et al., 2007), neovascularization at the pial surface (Drew et al., 2010), heartbeat pulsation-related movement artifacts (Paukert and Bergles, 2012), improper hemodynamics (Drew et al., 2010),

neuroplasticity defects (Xu et al., 2007), impaired glymphatic flow (Plog et al., 2019), and cortical spreading depression (Chang et al., 2010). Heightened levels of reactive astrocytes and microglia with cytokines expression were found within the first 2-3 weeks after installation of an open skull cranial window for chronic optical imaging. This was found to alter hemodynamic and neuronal responses upon sensory stimulation even six weeks posterior to surgery (Park et al., 2019). Such experimental neuroinflammatory response could modify CNS diseases progression in animal models with genetic or behavioral vulnerabilities, and corrupt physiological measures. Skull thinning is a minimally invasive procedure recommended for longitudinal *in vivo* imaging practice because it lacks many of the side effects resulting from craniotomy (Harb et al., 2013). Although transcranial imaging presents limitations in terms of depth and resolution of imaging (Xu et al., 2007), it is recommended for investigating chronic disease trajectories with a neuroinflammatory component (Arango-Lievano et al., 2016).

We developed fast transcranial imaging of blood flow, up to 0.8 kHz compatible with cellular resolution to identify the sites of cells death and regeneration. Photobleaching, phototoxicity and sample heating were not limitations of transcranial epifluorescence microscopy. Full-frame imaging allowed tracking of RBC trajectories in a large vascular perfusion domain assuming corrections for the focal planes and motion artifacts. This is an advantage compared to the line scanning technique of illumination that lacks macroscopic scale and degrades the optical sectioning (Brakenhoff et al., 1996). However, background fluorescence due to illumination outside the focal plan is limiting the depth of imaging. Using such preparation, we detected blood flow through the skull in small vessels down to 100 µm deep in the cerebral cortex. Deeper imaging shall be attainable with the new generation of fast 2-photon microscope up to 1 kHz as recently described (Zhang et al., 2019). However, *in vivo* optical imaging, especially in the brain, is limited to observations in millimiter-cube preparations due to the scattering of incident photons by the skull and brain. The mismatch of impedance between the skull and underlying layers could distort images. Because ultrasound scatters much less than light in tissue, photoacoustic tomography and ultrasonic imaging overcome some of the limitations associated with deep tissue imaging but they lack cellular precision (Errico et al., 2015; Xia et al., 2014).

Fast imaging revealed different speeds of cells in the same vessels (see supplementary movie 1). Unlike RBC, leukocytes crawl on the vessel walls looking for sites with gaps of

pericyte vascular coverage for transmigration into the parenchyma (Proebstl et al., 2012; Wang et al., 2006). Interruption of flow could result from leukocyte plugging of the capillaries (Cruz Hernandez et al., 2019; Yata et al., 2014). We observed this phenomenon 23 times in 56 sites of pericyte retractions in the epileptic brain, which is consistent with the no-reflow due to pericytosis in ischemic vessels and after spreading depolarization (Hall et al., 2014; Hill et al., 2015). In contrast, we did not observe any vessel occlusions at 40 sites of pericyte additions in the epileptic brain.

We expect that combining full-frame, multi-focal and fast imaging of biological events will improve the visualization of cell regeneration across the complex topological organization of the neurogliovascular unit. The heterogeneity of the mural cells across the cerebrovascular topology is a good example of imaging requiring rapid acquisition in a large field of view with multiple focal plans across various time frames. The fact that glutamate evoked a contraction of arterioles after a dilation of downstream capillaries could represent a safe mechanism for directing flow in the downstream perfusion domain. Ca^{2+} waves signaling between pericytes on capillaries and SMC on upstream arterioles have been previously involved in coordinated moderation of vasoactivity in the vascular domain (Peppiatt et al., 2006). Such timing of responses to glutamate was impaired after seizures and partially restored after treatment with PDGF-BB (Arango-Lievano et al., 2018). Classically, it is anticipated that mural cells morphology is tailored to its position and function on the cerebrovasculature (Shih et al., 2012; Tsai et al., 2015). That is, arteriolar SMC are contractile cells that impact the robustness of the perfusion domain (Blinder et al., 2010; Hillman, 2014) whereas the capillary pericytes control neuronal homeostasis and survival by sustaining the bulk exchange of metabolites and gases between blood and brain (Whiteus et al., 2014). Venular mesh pericytes control the clearance of parenchymal wastes and immune functions across the BBB (Proebstl et al., 2012).

Conclusions and perspectives

Multimodal *in vivo* cellular imaging approach will aid address the emerging questions about the assembly of multiple cell types in the functional organization of the neurogliovascular unit in the healthy brain as well as in the pathophysiology of CNS diseases. What can be learned from the *in vivo* dynamics of the newly formed cells that integrate in the multicellular organization of the neurogliovascular unit? Is it clinically relevant to promote the assembly or the disassembly of

specific cell types in the neurogliovascular network? What specific molecular mechanisms underlie these dynamic processes? Pharmacological strategies for promoting the repair of cell-cell interfaces supporting the neurogliovascular network and for regenerating the barrier functions and perfusion control of the cerebrovasculature are already being tested. One major application for visualizing cellular regeneration in the neurogliovascular unit is functional rehabilitation after a stroke or CNS injury that requires the growth and assembly of vessels, mural cells and astrocytes to supply the nutrients and oxygen needed for neuronal re-wiring in the surviving neuronal circuits (Demuth et al., 2017; Geranmayeh et al., 2019). Trophic factors and guidance molecules organizing the newborn cells in the neurogliovascular unit are already valuable candidates for the clinic (Arango-Lievano et al., 2018; Sweeney et al., 2016; Sweeney et al., 2019).

Technical recommendations pertaining to *in vivo* optical imaging: First, it is preferable to perform experiments in awake or lightly sedated animals (Grutzendler and Nedergaard, 2019). Second, light stimulation > 5mW is sufficient to dilate vessels and change blood flow, a pitfall to some opto-stimulation protocols (Katase et al., 2011). Third, epochs of several seconds shall be recorded for measuring blood flow as small fluctuations in flow can occur at homeostasis (Kleinfeld et al., 1998). Recommendations for future study design are to combine transcranial *in vivo* optical imaging with transcranial acoustic tomography to obtain the microscopic precision needed to study cellular network functions across mesoscopic brain-wide territories with temporal resolution (Boido et al., 2019; Ovsepian et al., 2017; Sofroniew et al., 2016; Yao and Wang, 2014). Although the voxel size limit using transcranial sonic imaging techniques is not yet compatible with cellular/subcellular precision (Errico et al., 2015; Osmanski et al., 2014), its rapid acquisition time and brain wide scale have great prospects for preclinical studies in primates and towards human brain imaging (Yan et al., 2020). Moreover, label free measurement of blood flow, velocity, hematocrit and tissue oxygenation *in vivo* with multiphoton high-resolution imaging would allow sophisticated investigation of brain microvascular flow regulation in CNS diseases and reveal underlying mechanisms (Guevara-Torres et al., 2016).

CRediT authorship contribution statement

Conceptualization (FJ, MAL); Formal analysis (MAL, PF, YD); Funding acquisition (MAL, FJ, PM); Investigation (FJ, MAL, YD); Methodology (CL, MAL, PF); Project administration (FJ,

MAL); Resources (FJ, PM); Software (PF); Roles/Writing - original draft (FJ); Writing - review & editing (MAL, PM, CL).

Declarations of Competing Interest

None

Acknowledgements

This work is supported by Ligue Française contre l'epilepsie (MA-L), Fondation pour la Recherche sur le Cerveau (FJ), France Alzheimer (FJ), IPAM-BioCampus Montpellier (PF, CL, PM) and FranceBioImaging ANR-10-INSB-04 (PM).

References

Abbott NJ, Ronnback L, Hansson E. Astrocyte-endothelial interactions at the blood-brain barrier. Nature reviews. Neuroscience, 2006; 7: 41-53.

Andrasfalvy BK, Zemelman BV, Tang J, Vaziri A. Two-photon single-cell optogenetic control of neuronal activity by sculpted light. Proceedings of the National Academy of Sciences of the United States of America, 2010; 107: 11981-6.

Arango-Lievano M, Borie AM, Dromard Y, Murat M, Desarmenien MG, Garabedian MJ, Jeanneteau F. Persistence of learning-induced synapses depends on neurotrophic priming of glucocorticoid receptors. Proceedings of the National Academy of Sciences of the United States of America, 2019; 116: 13097-106.

Arango-Lievano M, Boussadia B, De Terdonck LDT, Gault C, Fontanaud P, Lafont C, Mollard P, Marchi N, Jeanneteau F. Topographic Reorganization of Cerebrovascular Mural Cells under Seizure Conditions. Cell Rep, 2018; 23: 1045-59.

Arango-Lievano M, Giannoni P, Claeysen S, Marchi N, Jeanneteau F. Longitudinal In Vivo Imaging of the Cerebrovasculature: Relevance to CNS Diseases. J Vis Exp, 2016.

Armulik A, Genove G, Betsholtz C. Pericytes: developmental, physiological, and pathological perspectives, problems, and promises. Dev Cell, 2011; 21: 193-215.

Armulik A, Genove G, Mae M, Nisancioglu MH, Wallgard E, Niaudet C, He L, Norlin J, Lindblom P, Strittmatter K, Johansson BR, Betsholtz C. Pericytes regulate the blood-brain barrier. Nature, 2010; 468: 557-61.

Bell RD, Winkler EA, Sagare AP, Singh I, LaRue B, Deane R, Zlokovic BV. Pericytes control key neurovascular functions and neuronal phenotype in the adult brain and during brain aging. Neuron, 2010; 68: 409-27.

Ben-Ari Y. Kainate and Temporal Lobe Epilepsies: 3 decades of progress. In Noebels JL, Avoli M, Rogawski MA, Olsen RW, Delgado-Escueta AV, editors. Jasper's Basic Mechanisms of the Epilepsies: Bethesda (MD), 2012.

Berthiaume AA, Grant RI, McDowell KP, Underly RG, Hartmann DA, Levy M, Bhat NR, Shih AY. Dynamic Remodeling of Pericytes In Vivo Maintains Capillary Coverage in the Adult Mouse Brain. Cell Rep, 2018; 22: 8-16.

Blinder P, Shih AY, Rafie C, Kleinfeld D. Topological basis for the robust distribution of blood to rodent neocortex. Proceedings of the National Academy of Sciences of the United States of America, 2010; 107: 12670-5.
Boido D, Rungta RL, Osmanski BF, Roche M, Tsurugizawa T, Le Bihan D, Ciobanu L, Charpak S. Mesoscopic and microscopic imaging of sensory responses in the same animal. Nat Commun, 2019; 10: 1110.
Brakenhoff GJ, Squier J, Norris T, Bliton AC, Wade MH, Athey B. Real-time two-photon confocal microscopy using a femtosecond, amplified Ti:sapphire system. J Microsc, 1996; 181: 253-9.
Braun A, Xu H, Hu F, Kocherlakota P, Siegel D, Chander P, Ungvari Z, Csiszar A, Nedergaard M, Ballabh P. Paucity of pericytes in germinal matrix vasculature of premature infants. The Journal of neuroscience : the official journal of the Society for Neuroscience, 2007; 27: 12012-24.
Chang JC, Shook LL, Biag J, Nguyen EN, Toga AW, Charles AC, Brennan KC. Biphasic direct current shift, haemoglobin desaturation and neurovascular uncoupling in cortical spreading depression. Brain, 2010; 133: 996-1012.
Coelho-Santos V, Shih AY. Postnatal development of cerebrovascular structure and the neurogliovascular unit. Wiley Interdiscip Rev Dev Biol, 2020; 9: e363.
Cole JT, Yarnell A, Kean WS, Gold E, Lewis B, Ren M, McMullen DC, Jacobowitz DM, Pollard HB, O'Neill JT, Grunberg NE, Dalgard CL, Frank JA, Watson WD. Craniotomy: true sham for traumatic brain injury, or a sham of a sham? J Neurotrauma, 2011; 28: 359-69.
Cruz Hernandez JC, Bracko O, Kersbergen CJ, Muse V, Haft-Javaherian M, Berg M, Park L, Vinarcsik LK, Ivasyk I, Rivera DA, Kang Y, Cortes-Canteli M, Peyrounette M, Doyeux V, Smith A, Zhou J, Otte G, Beverly JD, Davenport E, Davit Y, Lin CP, Strickland S, Iadecola C, Lorthois S, Nishimura N, Schaffer CB. Neutrophil adhesion in brain capillaries reduces cortical blood flow and impairs memory function in Alzheimer's disease mouse models. Nature neuroscience, 2019; 22: 413-20.
Damisah EC, Hill RA, Tong L, Murray KN, Grutzendler J. A fluoro-Nissl dye identifies pericytes as distinct vascular mural cells during in vivo brain imaging. Nature neuroscience, 2017.
Daneman R, Zhou L, Kebede AA, Barres BA. Pericytes are required for blood-brain barrier integrity during embryogenesis. Nature, 2010; 468: 562-6.
Dehouck MP, Vigne P, Torpier G, Breittmayer JP, Cecchelli R, Frelin C. Endothelin-1 as a mediator of endothelial cell-pericyte interactions in bovine brain capillaries. Journal of cerebral blood flow and metabolism : official journal of the International Society of Cerebral Blood Flow and Metabolism, 1997; 17: 464-9.
Demuth HU, Dijkhuizen RM, Farr TD, Gelderblom M, Horsburgh K, Iadecola C, McLeod DD, Michalski D, Murphy TH, Orbe J, Otte WM, Petzold GC, Plesnila N, Reiser G, Reymann KG, Rueger MA, Saur D, Savitz SI, Schilling S, Spratt NJ, Turner RJ, Vemuganti R, Vivien D, Yepes M, Zille M, Boltze J, Isn, contributors Nm. Recent progress in translational research on neurovascular and neurodegenerative disorders. Restor Neurol Neurosci, 2017; 35: 87-103.
Di Giovanna AP, Tibo A, Silvestri L, Mullenbroich MC, Costantini I, Allegra Mascaro AL, Sacconi L, Frasconi P, Pavone FS. Whole-Brain Vasculature Reconstruction at the Single Capillary Level. Sci Rep, 2018; 8: 12573.

Drew PJ, Shih AY, Driscoll JD, Knutsen PM, Blinder P, Davalos D, Akassoglou K, Tsai PS, Kleinfeld D. Chronic optical access through a polished and reinforced thinned skull. Nat Methods, 2010; 7: 981-4.
Errico C, Pierre J, Pezet S, Desailly Y, Lenkei Z, Couture O, Tanter M. Ultrafast ultrasound localization microscopy for deep super-resolution vascular imaging. Nature, 2015; 527: 499-502.
Fenrich KK, Weber P, Hocine M, Zalc M, Rougon G, Debarbieux F. Long-term in vivo imaging of normal and pathological mouse spinal cord with subcellular resolution using implanted glass windows. J Physiol, 2012; 590: 3665-75.
Fernandez-Klett F, Potas JR, Hilpert D, Blazej K, Radke J, Huck J, Engel O, Stenzel W, Genove G, Priller J. Early loss of pericytes and perivascular stromal cell-induced scar formation after stroke. Journal of cerebral blood flow and metabolism : official journal of the International Society of Cerebral Blood Flow and Metabolism, 2013; 33: 428-39.
Foo SS, Turner CJ, Adams S, Compagni A, Aubyn D, Kogata N, Lindblom P, Shani M, Zicha D, Adams RH. Ephrin-B2 controls cell motility and adhesion during blood-vessel-wall assembly. Cell, 2006; 124: 161-73.
Gaengel K, Genove G, Armulik A, Betsholtz C. Endothelial-mural cell signaling in vascular development and angiogenesis. Arterioscler Thromb Vasc Biol, 2009; 29: 630-8.
Geranmayeh MH, Rahbarghazi R, Farhoudi M. Targeting pericytes for neurovascular regeneration. Cell Commun Signal, 2019; 17: 26.
Ghosh M, Balbi M, Hellal F, Dichgans M, Lindauer U, Plesnila N. Pericytes are involved in the pathogenesis of cerebral autosomal dominant arteriopathy with subcortical infarcts and leukoencephalopathy. Ann Neurol, 2015; 78: 887-900.
Giannoni P, Arango-Lievano M, Neves ID, Rousset MC, Baranger K, Rivera S, Jeanneteau F, Claeysen S, Marchi N. Cerebrovascular pathology during the progression of experimental Alzheimer's disease. Neurobiology of disease, 2016; 88: 107-17.
Grutzendler J, Nedergaard M. Cellular Control of Brain Capillary Blood Flow: In Vivo Imaging Veritas. Trends Neurosci, 2019; 42: 528-36.
Guevara-Torres A, Joseph A, Schallek JB. Label free measurement of retinal blood cell flux, velocity, hematocrit and capillary width in the living mouse eye. Biomed Opt Express, 2016; 7: 4228-49.
Hall CN, Reynell C, Gesslein B, Hamilton NB, Mishra A, Sutherland BA, O'Farrell FM, Buchan AM, Lauritzen M, Attwell D. Capillary pericytes regulate cerebral blood flow in health and disease. Nature, 2014; 508: 55-60.
Harb R, Whiteus C, Freitas C, Grutzendler J. In vivo imaging of cerebral microvascular plasticity from birth to death. Journal of cerebral blood flow and metabolism : official journal of the International Society of Cerebral Blood Flow and Metabolism, 2013; 33: 146-56.
Harris JJ, Jolivet R, Attwell D. Synaptic energy use and supply. Neuron, 2012; 75: 762-77.
He L, Vanlandewijck M, Raschperger E, Andaloussi Mae M, Jung B, Lebouvier T, Ando K, Hofmann J, Keller A, Betsholtz C. Analysis of the brain mural cell transcriptome. Scientific reports, 2016; 6: 35108.
Hill RA, Grutzendler J. In vivo imaging of oligodendrocytes with sulforhodamine 101. Nat Methods, 2014; 11: 1081-2.

Hill RA, Tong L, Yuan P, Murikinati S, Gupta S, Grutzendler J. Regional Blood Flow in the Normal and Ischemic Brain Is Controlled by Arteriolar Smooth Muscle Cell Contractility and Not by Capillary Pericytes. Neuron, 2015; 87: 95-110.
Hillman EM. Coupling mechanism and significance of the BOLD signal: a status report. Annu Rev Neurosci, 2014; 37: 161-81.
Hulsmann S, Hagos L, Heuer H, Schnell C. Limitations of Sulforhodamine 101 for Brain Imaging. Front Cell Neurosci, 2017; 11: 44.
Iadecola C. The Neurovascular Unit Coming of Age: A Journey through Neurovascular Coupling in Health and Disease. Neuron, 2017; 96: 17-42.
Iadecola C. The pathobiology of vascular dementia. Neuron, 2013; 80: 844-66.
Iadecola C, Yang G, Ebner TJ, Chen G. Local and propagated vascular responses evoked by focal synaptic activity in cerebellar cortex. J Neurophysiol, 1997; 78: 651-9.
Iliff JJ, Chen MJ, Plog BA, Zeppenfeld DM, Soltero M, Yang L, Singh I, Deane R, Nedergaard M. Impairment of glymphatic pathway function promotes tau pathology after traumatic brain injury. J Neurosci, 2014; 34: 16180-93.
Katase T, Ishimaru Y, Tsukamoto A, Hiramatsu H, Kamiya T, Tanabe K, Hosono H. Advantageous grain boundaries in iron pnictide superconductors. Nat Commun, 2011; 2: 409.
Kim TN, Goodwill PW, Chen Y, Conolly SM, Schaffer CB, Liepmann D, Wang RA. Line-scanning particle image velocimetry: an optical approach for quantifying a wide range of blood flow speeds in live animals. PLoS One, 2012; 7: e38590.
Kisler K, Nelson AR, Rege SV, Ramanathan A, Wang Y, Ahuja A, Lazic D, Tsai PS, Zhao Z, Zhou Y, Boas DA, Sakadzic S, Zlokovic BV. Pericyte degeneration leads to neurovascular uncoupling and limits oxygen supply to brain. Nat Neurosci, 2017; 20: 406-16.
Kisler K, Nikolakopoulou AM, Sweeney M, Zlokovic B. Acute Ablation of Cortical Pericytes Leads to Rapid Neurovascular Uncoupling. Frontiers in Cellular Neuroscience, 2020; 14.
Kleinfeld D, Mitra PP, Helmchen F, Denk W. Fluctuations and stimulus-induced changes in blood flow observed in individual capillaries in layers 2 through 4 of rat neocortex. Proc Natl Acad Sci U S A, 1998; 95: 15741-6.
Kumar A, D'Souza SS, Moskvin OV, Toh H, Wang B, Zhang J, Swanson S, Guo LW, Thomson JA, Slukvin, II. Specification and Diversification of Pericytes and Smooth Muscle Cells from Mesenchymoangioblasts. Cell Rep, 2017; 19: 1902-16.
Lafont C, Desarmenien MG, Cassou M, Molino F, Lecoq J, Hodson D, Lacampagne A, Mennessier G, El Yandouzi T, Carmignac D, Fontanaud P, Christian H, Coutry N, Fernandez-Fuente M, Charpak S, Le Tissier P, Robinson IC, Mollard P. Cellular in vivo imaging reveals coordinated regulation of pituitary microcirculation and GH cell network function. Proceedings of the National Academy of Sciences of the United States of America, 2010; 107: 4465-70.
Lagraoui M, Latoche JR, Cartwright NG, Sukumar G, Dalgard CL, Schaefer BC. Controlled cortical impact and craniotomy induce strikingly similar profiles of inflammatory gene expression, but with distinct kinetics. Front Neurol, 2012; 3: 155.
Leal-Campanario R, Alarcon-Martinez L, Rieiro H, Martinez-Conde S, Alarcon-Martinez T, Zhao X, LaMee J, Popp PJ, Calhoun ME, Arribas JI, Schlegel AA, Stasi LL, Rho JM, Inge L, Otero-Millan J, Treiman DM, Macknik SL. Abnormal Capillary Vasodynamics Contribute to Ictal Neurodegeneration in Epilepsy. Sci Rep, 2017; 7: 43276.

Lendahl U, Nilsson P, Betsholtz C. Emerging links between cerebrovascular and neurodegenerative diseases-a special role for pericytes. EMBO Rep, 2019; 20: e48070.
Li H, Yan M, Yu J, Xu Q, Xia X, Liao J, Zheng W. In vivo identification of arteries and veins using two-photon excitation elastin autofluorescence. J Anat, 2020; 236: 171-9.
Maki T, Hayakawa K, Pham LD, Xing C, Lo EH, Arai K. Biphasic mechanisms of neurovascular unit injury and protection in CNS diseases. CNS Neurol Disord Drug Targets, 2013; 12: 302-15.
Mateo C, Knutsen PM, Tsai PS, Shih AY, Kleinfeld D. Entrainment of Arteriole Vasomotor Fluctuations by Neural Activity Is a Basis of Blood-Oxygenation-Level-Dependent "Resting-State" Connectivity. Neuron, 2017; 96: 936-48 e3.
Montagne A, Barnes SR, Sweeney MD, Halliday MR, Sagare AP, Zhao Z, Toga AW, Jacobs RE, Liu CY, Amezcua L, Harrington MG, Chui HC, Law M, Zlokovic BV. Blood-brain barrier breakdown in the aging human hippocampus. Neuron, 2015; 85: 296-302.
Montagne A, Nikolakopoulou AM, Zhao Z, Sagare AP, Si G, Lazic D, Barnes SR, Daianu M, Ramanathan A, Go A, Lawson EJ, Wang Y, Mack WJ, Thompson PM, Schneider JA, Varkey J, Langen R, Mullins E, Jacobs RE, Zlokovic BV. Pericyte degeneration causes white matter dysfunction in the mouse central nervous system. Nat Med, 2018; 24: 326-37.
Nikolakopoulou AM, Montagne A, Kisler K, Dai Z, Wang Y, Huuskonen MT, Sagare AP, Lazic D, Sweeney MD, Kong P, Wang M, Owens NC, Lawson EJ, Xie X, Zhao Z, Zlokovic BV. Pericyte loss leads to circulatory failure and pleiotrophin depletion causing neuron loss. Nat Neurosci, 2019; 22: 1089-98.
Ogura S, Kurata K, Hattori Y, Takase H, Ishiguro-Oonuma T, Hwang Y, Ahn S, Park I, Ikeda W, Kusuhara S, Fukushima Y, Nara H, Sakai H, Fujiwara T, Matsushita J, Ema M, Hirashima M, Minami T, Shibuya M, Takakura N, Kim P, Miyata T, Ogura Y, Uemura A. Sustained inflammation after pericyte depletion induces irreversible blood-retina barrier breakdown. JCI Insight, 2017; 2: e90905.
Osmanski BF, Pezet S, Ricobaraza A, Lenkei Z, Tanter M. Functional ultrasound imaging of intrinsic connectivity in the living rat brain with high spatiotemporal resolution. Nat Commun, 2014; 5: 5023.
Ovsepian SV, Olefir I, Westmeyer G, Razansky D, Ntziachristos V. Pushing the Boundaries of Neuroimaging with Optoacoustics. Neuron, 2017; 96: 966-88.
Park DY, Lee J, Kim J, Kim K, Hong S, Han S, Kubota Y, Augustin HG, Ding L, Kim JW, Kim H, He Y, Adams RH, Koh GY. Plastic roles of pericytes in the blood-retinal barrier. Nat Commun, 2017; 8: 15296.
Park H, You N, Lee J, Suh M. Longitudinal study of hemodynamics and dendritic membrane potential changes in the mouse cortex following a soft cranial window installation. Neurophotonics, 2019; 6: 015006.
Paukert M, Bergles DE. Reduction of motion artifacts during in vivo two-photon imaging of brain through heartbeat triggered scanning. J Physiol, 2012; 590: 2955-63.
Peppiatt CM, Howarth C, Mobbs P, Attwell D. Bidirectional control of CNS capillary diameter by pericytes. Nature, 2006; 443: 700-4.
Plog BA, Lou N, Pierre CA, Cove A, Kenney HM, Hitomi E, Kang H, Iliff JJ, Zeppenfeld DM, Nedergaard M, Vates GE. When the air hits your brain: decreased arterial pulsatility after craniectomy leading to impaired glymphatic flow. J Neurosurg, 2019: 1-14.

Proebstl D, Voisin MB, Woodfin A, Whiteford J, D'Acquisto F, Jones GE, Rowe D, Nourshargh S. Pericytes support neutrophil subendothelial cell crawling and breaching of venular walls in vivo. J Exp Med, 2012; 209: 1219-34.
Rasmussen MK, Mestre H, Nedergaard M. The glymphatic pathway in neurological disorders. Lancet Neurol, 2018; 17: 1016-24.
Rustenhoven J, Jansson D, Smyth LC, Dragunow M. Brain Pericytes As Mediators of Neuroinflammation. Trends Pharmacol Sci, 2017; 38: 291-304.
Sagare AP, Bell RD, Zhao Z, Ma Q, Winkler EA, Ramanathan A, Zlokovic BV. Pericyte loss influences Alzheimer-like neurodegeneration in mice. Nat Commun, 2013; 4: 2932.
Salvucci O, Maric D, Economopoulou M, Sakakibara S, Merlin S, Follenzi A, Tosato G. EphrinB reverse signaling contributes to endothelial and mural cell assembly into vascular structures. Blood, 2009; 114: 1707-16.
Shen Z, Lu Z, Chhatbar PY, O'Herron P, Kara P. An artery-specific fluorescent dye for studying neurovascular coupling. Nat Methods, 2012; 9: 273-6.
Shibahara T, Ago T, Nakamura K, Tachibana M, Yoshikawa Y, Komori M, Yamanaka K, Wakisaka Y, Kitazono T. Pericyte-mediated tissue repair through PDGFRbeta promotes peri-infarct astrogliosis, oligodendrogenesis and functional recovery after acute ischemic stroke. eNeuro, 2020.
Shih AY, Driscoll JD, Drew PJ, Nishimura N, Schaffer CB, Kleinfeld D. Two-photon microscopy as a tool to study blood flow and neurovascular coupling in the rodent brain. J Cereb Blood Flow Metab, 2012; 32: 1277-309.
Sofroniew NJ, Flickinger D, King J, Svoboda K. A large field of view two-photon mesoscope with subcellular resolution for in vivo imaging. Elife, 2016; 5.
Stanimirovic DB, Friedman A. Pathophysiology of the neurovascular unit: disease cause or consequence? Journal of cerebral blood flow and metabolism : official journal of the International Society of Cerebral Blood Flow and Metabolism, 2012; 32: 1207-21.
Sweeney MD, Ayyadurai S, Zlokovic BV. Pericytes of the neurovascular unit: key functions and signaling pathways. Nature neuroscience, 2016; 19: 771-83.
Sweeney MD, Zhao Z, Montagne A, Nelson AR, Zlokovic BV. Blood-Brain Barrier: From Physiology to Disease and Back. Physiol Rev, 2019; 99: 21-78.
Tedeschi A, Dupraz S, Laskowski CJ, Xue J, Ulas T, Beyer M, Schultze JL, Bradke F. The Calcium Channel Subunit Alpha2delta2 Suppresses Axon Regeneration in the Adult CNS. Neuron, 2016; 92: 419-34.
Trost A, Lange S, Schroedl F, Bruckner D, Motloch KA, Bogner B, Kaser-Eichberger A, Strohmaier C, Runge C, Aigner L, Rivera FJ, Reitsamer HA. Brain and Retinal Pericytes: Origin, Function and Role. Front Cell Neurosci, 2016; 10: 20.
Tsai PS, Mateo C, Field JJ, Schaffer CB, Anderson ME, Kleinfeld D. Ultra-large field-of-view two-photon microscopy. Opt Express, 2015; 23: 13833-47.
Vanlandewijck M, He L, Mae MA, Andrae J, Ando K, Del Gaudio F, Nahar K, Lebouvier T, Lavina B, Gouveia L, Sun Y, Raschperger E, Rasanen M, Zarb Y, Mochizuki N, Keller A, Lendahl U, Betsholtz C. A molecular atlas of cell types and zonation in the brain vasculature. Nature, 2018; 554: 475-80.
Wang S, Voisin MB, Larbi KY, Dangerfield J, Scheiermann C, Tran M, Maxwell PH, Sorokin L, Nourshargh S. Venular basement membranes contain specific matrix protein low expression regions that act as exit points for emigrating neutrophils. J Exp Med, 2006; 203: 1519-32.

Whiteus C, Freitas C, Grutzendler J. Perturbed neural activity disrupts cerebral angiogenesis during a postnatal critical period. Nature, 2014; 505: 407-11.
Winkler EA, Bell RD, Zlokovic BV. Central nervous system pericytes in health and disease. Nature neuroscience, 2011; 14: 1398-405.
Winkler EA, Sengillo JD, Sullivan JS, Henkel JS, Appel SH, Zlokovic BV. Blood-spinal cord barrier breakdown and pericyte reductions in amyotrophic lateral sclerosis. Acta Neuropathol, 2013; 125: 111-20.
Xia J, Yao J, Wang LV. Photoacoustic tomography: principles and advances. Electromagn Waves (Camb), 2014; 147: 1-22.
Xing C, Lo EH. Help-me signaling: Non-cell autonomous mechanisms of neuroprotection and neurorecovery. Prog Neurobiol, 2017; 152: 181-99.
Xu HT, Pan F, Yang G, Gan WB. Choice of cranial window type for in vivo imaging affects dendritic spine turnover in the cortex. Nature neuroscience, 2007; 10: 549-51.
Yan L, Zhou X, Yang X, Zheng Y, Liu C, Zheng L, Fang L, Luo W, He G, He J, Zheng J, Zhou Y. Establishment and Evaluation of a Monkey Acute Cerebral Ischemia Model. Clinics (Sao Paulo), 2020; 75: e1339.
Yao J, Wang LV. Photoacoustic Brain Imaging: from Microscopic to Macroscopic Scales. Neurophotonics, 2014; 1.
Yata K, Nishimura Y, Unekawa M, Tomita Y, Suzuki N, Tanaka T, Mizoguchi A, Tomimoto H. In vivo imaging of the mouse neurovascular unit under chronic cerebral hypoperfusion. Stroke, 2014; 45: 3698-703.
Zehendner CM, Sebastiani A, Hugonnet A, Bischoff F, Luhmann HJ, Thal SC. Traumatic brain injury results in rapid pericyte loss followed by reactive pericytosis in the cerebral cortex. Sci Rep, 2015; 5: 13497.
Zhang T, Hernandez O, Chrapkiewicz R, Shai A, Wagner MJ, Zhang Y, Wu CH, Li JZ, Inoue M, Gong Y, Ahanonu B, Zeng H, Bito H, Schnitzer MJ. Kilohertz two-photon brain imaging in awake mice. Nat Methods, 2019; 16: 1119-22.
Zhao Z, Nelson AR, Betsholtz C, Zlokovic BV. Establishment and Dysfunction of the Blood-Brain Barrier. Cell, 2015; 163: 1064-78.
Zlokovic BV. The blood-brain barrier in health and chronic neurodegenerative disorders. Neuron, 2008; 57: 178-201.

Figures and legends

Figure 1. Multimodal optical transcranial imaging as a diagnostic mode.

Follow up study of *NG2-tdTomato* transgenic mice before and after the induction of generalized seizures with a single i.p. injection of 25 mg/kg kainate, and following 3 weeks of treatment with i.v. injection of saline or 100 □g PDGF-BB per week. Control mice were injected with saline instead of kainate. Methodological timeline divided in 3 sessions of observational parameters of cellular integrity and function *in situ*: 1) healthy, 2) sick and 3) treated. At last, postmortem histological studies confirm brain wide tissue damage and repair.

Figure 2. Imaging the dynamic organization of the neurogliovascular unit *in vivo*.

(A) Genetic tracers and chemical dyes compatible with *in vivo* time lapse imaging of the multicellular interfaces in the neurogliovascular unit. 3D reconstruction of a neurogliovascular unit imaged with *thy1*-YFP, SR101 and 70 kDa dextran-FITC *in vivo* using transcranial 2-photon microscopy. 3D reconstruction of the topological distribution of mural cells on the cerebrovasculature imaged *in vivo* with *NG2*-tdTomato and 70 kDa dextran-FITC. SMC on arterioles can be distinguished with AlexaFluor 633-hydrazide. Capillary and post-capillary pericytes can be labeled with neurotrace™ and expression of genetic tracers with *Cnn1* and *Acta2, Tagln* promoters (Vanlandewijck et al., 2018). Capillaries and venules can be labeled with the genetic markers expressed under the control of *Ecm*, and *Abcc9* promoters (Vanlandewijck et al., 2018). 3D reconstruction of an interface between neurons and pericytes imaged *in vivo* with *thy1*-YFP and *NG2*-tdTomato. 3D reconstruction of an interface between astrocyte endfoot and an axon terminal on the vasculature imaged with *thy1*-YFP, SR101 and 70 kDa dextran-FITC *in vivo* using transcranial 2-photon microscopy. (B) Topological organization of a variety of mural cells morphologies tailored to the vessel subtypes.

Figure 3. Functional *in vivo* imaging of pericyte degeneration and regeneration.

(A) Transcranial 2-photon microscopy of the same microvessels a1 and a2 (70-kDa dextran-FITC) and pericytes (*NG2*-tdTomato) during a period of 8 weeks in the same mouse brain before and after seizure onset and treatment. Pericyte remodeling at 75 µm deep associated with changes of vessel diameter. (B) Transcranial epifluorescence microscopy of blood cells velocity at 75 µm deep into the cortex at the sites of pericyte retraction and extension. Arrows point to direction of flow and numbers to the speed of flow in arterioles (a1 and a2), capillaries (c) and venules (v). Flow is variable in vessel a1: backflow at the site of pericyte retraction after seizure induction accelerated flow in vessels a2, c and v. Later post-treatment, pericyte extension on vessel a1 normalized flow in all vessels. See movie 1 for transcranial flow imaging after seizure induction and movie 2 for transcranial flow imaging after the treatment. (C) Open skull 2-photon microscopy of the pericyte-vessel interface at 75 µm depth where pericyte regenerated on vessel a1 46 days post-treatment. See movie 3 and movie 4 for *in vivo* time-lapse responses of vessels a1, a2, v and c to 10^{-4} M glutamate and 10^{-8} M endothelin-1 applied topically via the cranial window and rinsed with ASCF. Kymographs represent vessel diameters at indicated cross-sections as a function of time for dextran-FITC and *NG2*-tdTomato cells. Data are plotted in the graph for each vessel.

Figure 4. Analysis of vasoactivity upon turnover of mural cells subtypes *in vivo*.

(A) Blood flow circulation in the vascular domain assisted by the coordinated contraction of arterioles and dilation of downstream capillaries. Mural cells determine the action domain of vasoactive molecules (*e.g.* ET-1 and GLU) thanks to their topology on the cerebrovasculature and various morphologies. (B) Net change of vessel diameter to vasoactive drugs where mural cells pre-existed or lacked from the first imaging session. Means ±SEM of N vessels as indicated in 3 mice. Two-way ANOVA for the effect of 10^{-8} M ET-1 on: vessel subtypes $F(2,137)=891.5$, $P<0.0001$; at sites of pericyte coverage $F(1,137)=54.1$, $P<0.0001$ and its interaction $F(2,137)=38.76$, $P<0.0001$. Two-way ANOVA for the effect of 10^{-4} M GLU on: vessel subtypes $F(2,137)=135.4$, $P<0.0001$; at sites of pericyte coverage $F(1,137)=5.66$, $P=0.018$ and its interaction $F(2,137)=27.1$, $P<0.0001$. Post-hoc Sidak test comparing vasoactivity on vessels with pericytes and vessels without pericytes $*P<0.05$, $**P<0.001$, $***P<0.0001$. (C) Comparison of vasoactivity on vessels gaining or loosing pericytes. Each vessel presented as a thin line before and after stimulation with vasoactive drugs. Thick lines represent the mean of N vessels indicated for each vessel categories. Capillaries with pericyte loss failed to dilate with GLU unlike vessels with newly formed pericytes. (D) How does the newly formed pericytes compare with the pre-existing ones or the vessels loosing pericytes compare with vessel never covered in term of vasoactivity? Two-way ANOVA for the effect of GLU on vessel subtypes $F(8,264)=74.9$, $P<0.0001$; at sites of pericyte turnover $F(1,264)=36.3$, $P<0.0001$; Effect of ET1 on vessel subtypes $F(8,264)=271.3$, $P<0.0001$; at sites of pericyte turnover $F(1,264)=9.64$, $P=0.0021$. Post-hoc comparisons with Tukey test are presented. SE of diff.= standard error of difference.

Figure 5. Analysis of blood flow upon turnover of mural cells subtypes *in vivo*.

(A) Transcranial epifluorescence microscopy show pulsatile flow of RBC in large caliber vessels. Average speed of flow is calculated from at least 2 s of *in vivo* recordings. (B) Average blood flow sorted by vessel subtypes defined by the morphology of its pericytes and its caliber at baseline (arterioles > 7 µm capillaries < venules). N= 30 arterioles, 44 capillaries and 68 venules from 3 healthy mice. Flow in arteriole > venules > capillaries by one-way ANOVA $F(2,139)=91$, $P<0.0001$ post-hoc Sidak test $P<0.0001$. (C) Flow in control mice indistinguishable between in vessels covered or not covered with pericytes: N= 10 arterioles, 10 capillaries and 19 venules covered with pre-existing mural cells and 18 arterioles, 26 capillaries and 27 venules without pericytes. One-way ANOVA $F(5,104)=18.38$, $P<0.0001$ post-hoc Sidak test $P>0.5$. Hyperemia in capillaries with pericytes loss after seizures treated with saline: N= 8 arterioles, 15 capillaries and 9 venules covered with pre-existing mural cells; 5 arterioles, 18 capillaries and 22 venules not covered; 3 arterioles, 4 capillaries and 7 venules with a pericyte gain; 8 arterioles, 13 capillaries and 12 venules with pericyte loss. One-way ANOVA $F(11,112)=3.11$, $P=0.001$ post-hoc Sidak test $P=0.003$. Alterations of flow after treatment of seizures with PDGF-BB at residual sites of pericyte loss: N= 9 arterioles, 45 capillaries and 12 venules covered with pre-existing mural cells; 9 arterioles, 33 capillaries and 9 venules not covered; 10 arterioles, 7 capillaries and 9 venules with a pericyte gain; 4 arterioles, 4 capillaries and 5 venules with pericyte loss. One-way ANOVA $F(11,144)=10.64$, $P<0.0001$ post-hoc Sidak test $P=0.0007$. (D) Balancing effect of pericyte turnover on blood flow. If seizures are treated with saline, pericyte loss reduces local flow, which could cause hyperemia in neighboring perfusion domains despite some pericyte gains. If seizures are treated with PDGF-BB, gains of pericytes offset the losses thereby normalizing flow in the perfusion domain. (E) Branch-specific changes of vessel perfusion correspond with pericyte retraction and extension. Images are representative of 23 occlusions observed at 56 sites of pericyte loss and 0 occlusions observed at 40 sites of pericyte gain. Z-stacks of the indicated cross-sections at vessel bifurcations are showed sideways. Numbers indicate the order of vessels following to direction of flow represented by arrows.

Figure 6. Analysis post-mortem of vessel permeability and pericyte death and proliferation. (A-C) Angiogram with the permeable dye 10 Kda dextran-Alexa568 injected i.v. before sacrifice shows extravasation from the lumen into cells of the neurovascular unit at bifurcations between vessels covered with pericytes labeled with PDGFRβ (1:100, Abcam ab32570). Images a representative of N=41 bifurcation in capillaries, 17 in arterioles and 26 in venules of 11 mice. (D, E) Capillary pericytes labeled with the apoptotic marker cleaved caspase-3 (1:100, Cell Signaling Technologies) or with the proliferation marker KI-67 (1:500 Abcam ab15580) at vessels bifurcations. Images a representative of N=15 pericytes with CC3 and 16 pericytes with KI67 in 11 mice. Images were taken in a field of 150 μm x 150 μm at 0.75 μm step in z with a confocal microscope LSM780 (Carl Zeiss) and 20x water immersion objective. Z-stacks of the indicated cross-sections at vessel bifurcations are showed sideways. Numbers indicate the order of vessels following to direction of flow.

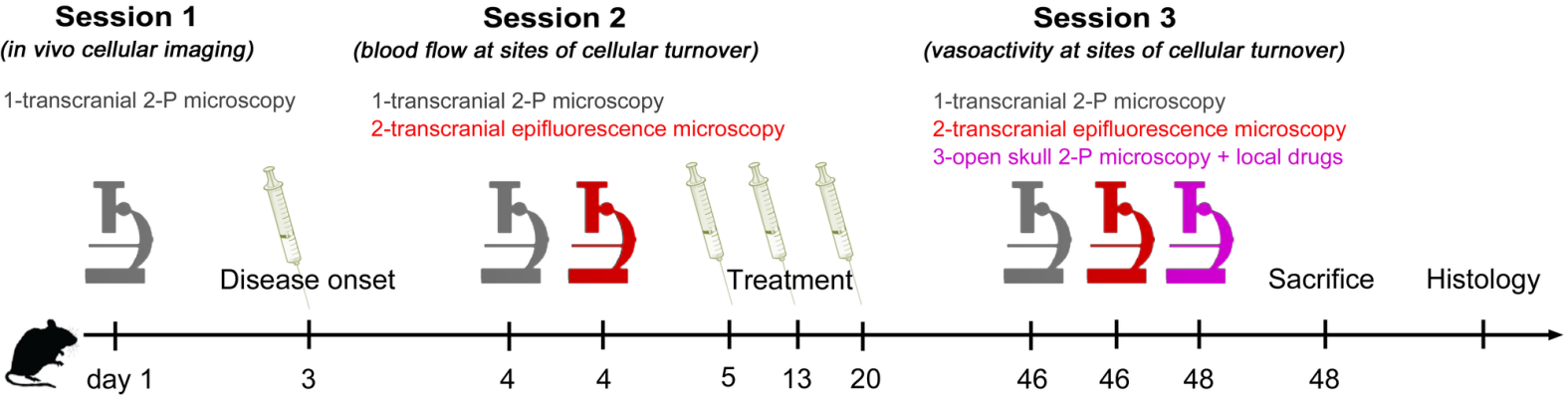
Session 1
(in vivo cellular imaging)
1-transcranial 2-P microscopy
Session 2
(blood flow at sites of cellular turnover)
1-transcranial 2-P microscopy
2-transcranial epifluorescence microscopy
Session 3
(vasoactivity at sites of cellular turnover)
1-transcranial 2-P microscopy
2-transcranial epifluorescence microscopy
3-open skull 2-P microscopy + local drugs
Disease onset
Treatment
Sacrifice
Histology
day 1
3
4
4
5
13
20
46
46
48
48

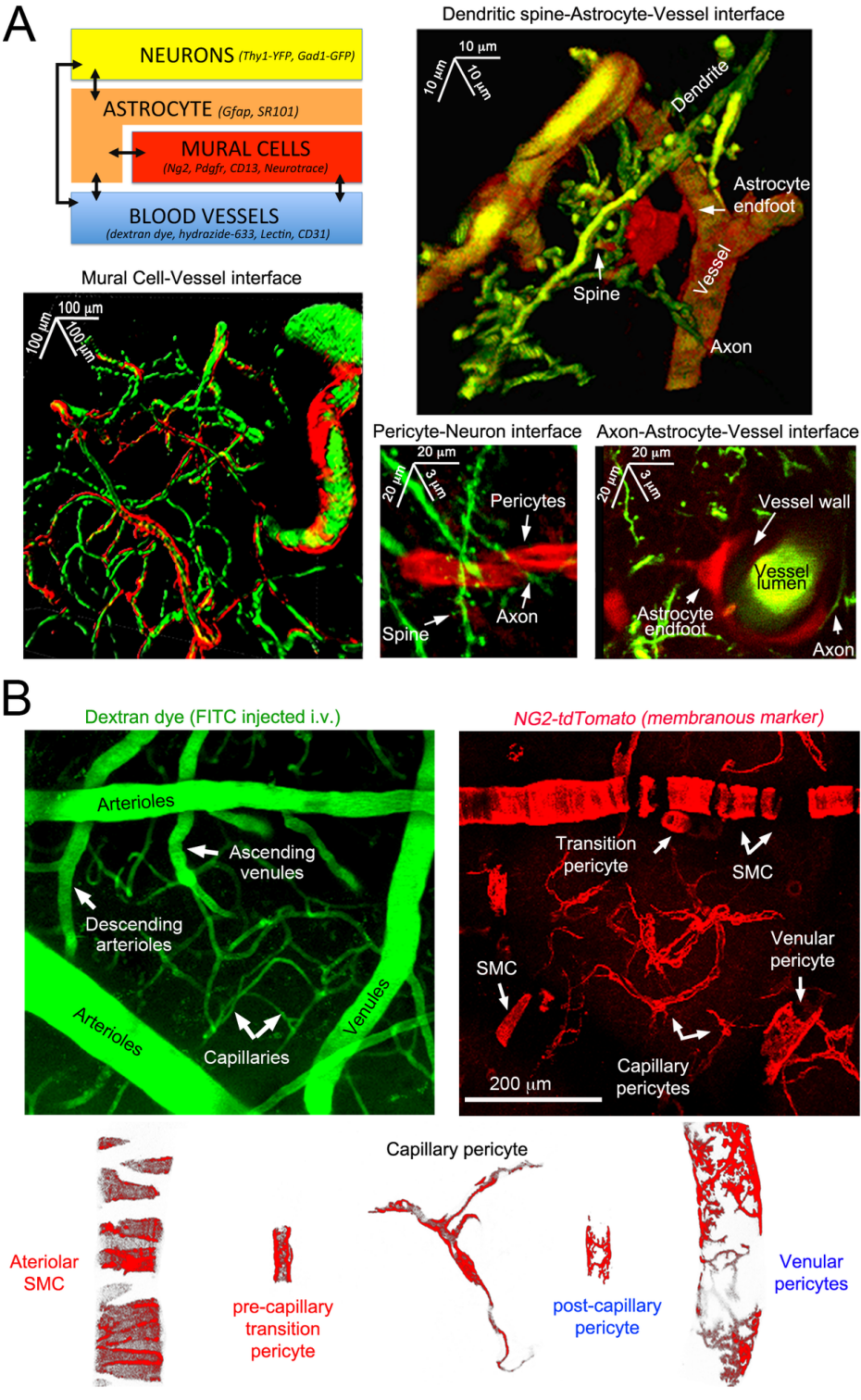
A
NEURONS (Thy1-YFP, Gad1-GFP)
ASTROCYTE (Gfap, SR101)
MURAL CELLS
(Ng2, Pdgfr, CD13, Neurotrace)
BLOOD VESSELS
(dextran dye, hydrazide-633, Lectin, CD31)
Dendritic spine-Astrocyte-Vessel interface
10 μm
10 μm
10 μm
Dendrite
Astrocyte endfoot
Vessel
Spine
Axon
Mural Cell-Vessel interface
100 μm
100 μm
100 μm
Pericyte-Neuron interface
20 μm
20 μm
3 μm
Pericytes
Axon
Spine
Axon-Astrocyte-Vessel interface
20 μm
20 μm
3 μm
Vessel wall
Vessel lumen
Astrocyte endfoot
Axon
B
Dextran dye (FITC injected i.v.)
Arterioles
Ascending venules
Descending arterioles
Arterioles
Capillaries
Venules
NG2-tdTomato (membranous marker)
Transition pericyte
SMC
SMC
Venular pericyte
Capillary pericytes
200 μm
Capillary pericyte
Ateriolar SMC
pre-capillary transition pericyte
post-capillary pericyte
Venular pericytes

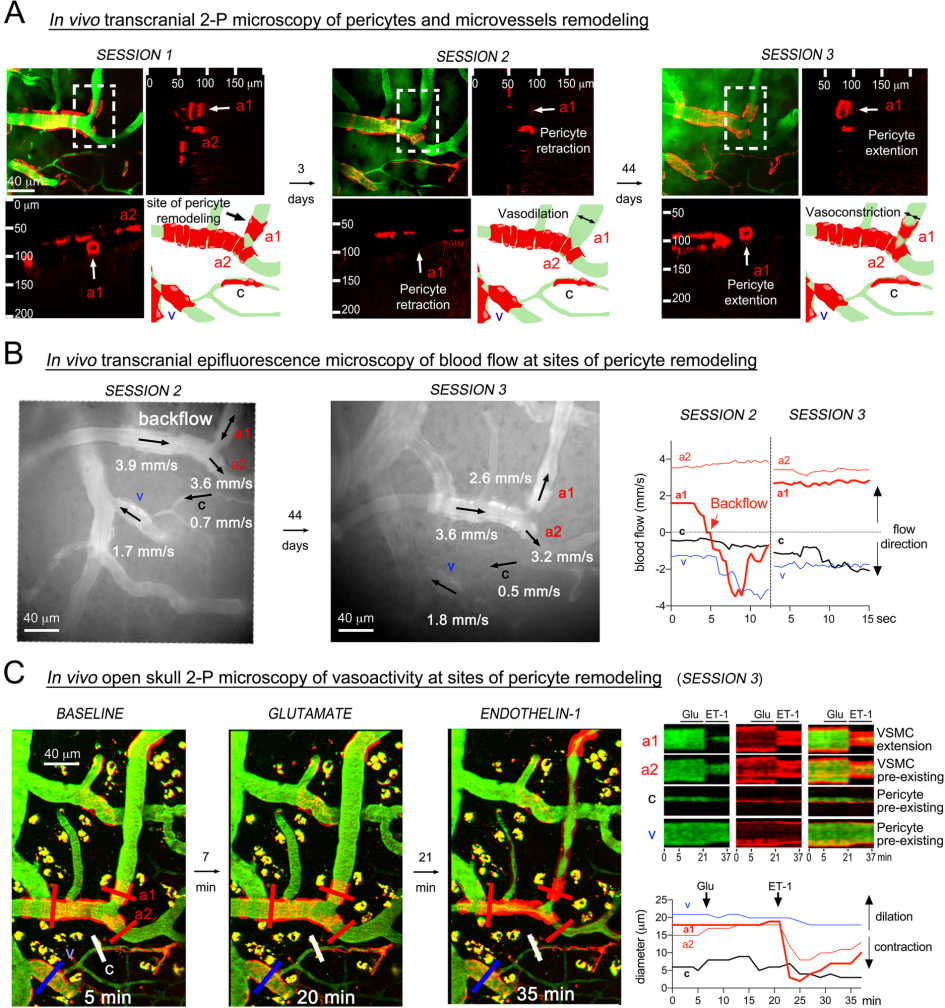
A
In vivo transcranial 2-P microscopy of pericytes and microvessels remodeling
SESSION 1
SESSION 2
SESSION 3
3 days
44 days
a1
a2
c
v
40 µm
Pericyte retraction
Pericyte extention
site of pericyte remodeling
Vasodilation
Vasoconstriction
B
In vivo transcranial epifluorescence microscopy of blood flow at sites of pericyte remodeling
SESSION 2
SESSION 3
backflow
3.9 mm/s
3.6 mm/s
0.7 mm/s
1.7 mm/s
2.6 mm/s
3.6 mm/s
3.2 mm/s
0.5 mm/s
1.8 mm/s
44 days
Backflow
blood flow (mm/s)
flow direction
sec
C
In vivo open skull 2-P microscopy of vasoactivity at sites of pericyte remodeling (SESSION 3)
BASELINE
GLUTAMATE
ENDOTHELIN-1
7 min
21 min
5 min
20 min
35 min
Glu
ET-1
VSMC extension
VSMC pre-existing
Pericyte pre-existing
Pericyte pre-existing
dilation
contraction
diameter (µm)
min

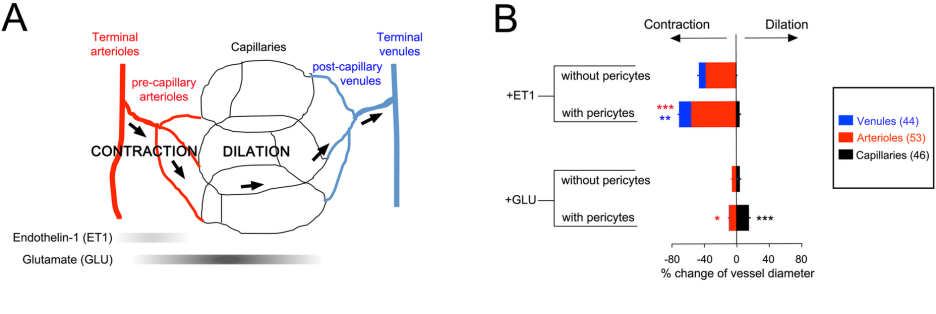

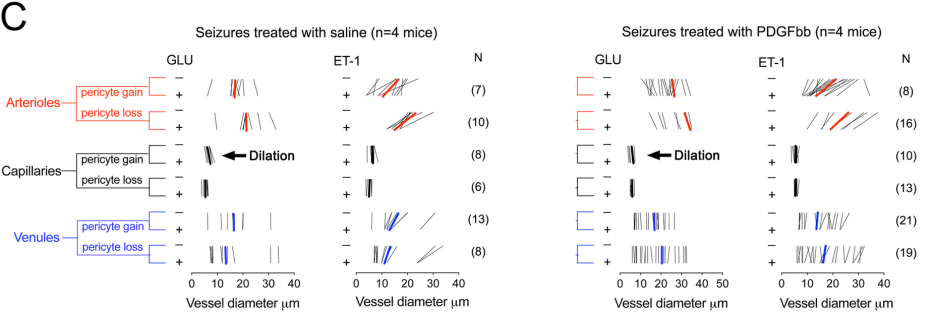

D

Vessel type	Comparisons between mouse groups	Comparisons between cell types	Effect of GLU			Effect of ET1		
			Mean diff.	*SE of diff.*	*P value*	*Mean diff.*	*SE of diff.*	*P value*
Arterioles	Controls vs.Seizures+saline	New pericyte vs. Pre-exisiting pericyte	-8.1	1.51	<0.0001 ***	-19.7	2.39	<0.0001 ***
		Lost pericyte vs. No pericyte	-6.0	1.70	0.0193 *	-2.1	2.70	0.9972
	Controls vs.Seizures+PDGFbb	New pericyte vs. Pre-exisiting pericyte	-13.5	1.29	<0.0001 ***	-19.7	2.05	<0.0001 ***
		Lost pericyte vs. No pericyte	-14.2	1.62	<0.0001 ***	-11.3	2.56	0.0005 **
	Seizures+saline vs.Seizures+PDGFbb	New pericyte vs. New pericyte+PDGFbb	-5.4	1.62	0.0359 *	0.1	2.58	>0.9999
		Lost pericyte vs. Lost pericyte+PDGFbb	-8.2	2.09	0.0038 *	-9.1	3.31	0.1314
Capillaries	Controls vs.Seizures+saline	New pericyte vs. Pre-exisiting pericyte	-4.1	1.82	0.5843	0.3	2.89	>0.9999
		Lost pericyte vs. No pericyte	1.7	1.70	>0.9999	5.0	2.70	0.637
	Controls vs.Seizures+PDGFbb	New pericyte vs. Pre-exisiting pericyte	2.6	1.36	0.8862	2.3	2.16	0.9781
		Lost pericyte vs. No pericyte	3.4	1.57	0.6823	3.7	2.50	0.8564
	Seizures+saline vs.Seizures+PDGFbb	New pericyte vs. New pericyte+PDGFbb	6.7	1.99	0.0302 *	2.1	3.16	0.9993
		Lost pericyte vs. Lost pericyte+PDGFbb	1.7	1.91	>0.9999	-1.3	3.03	>0.9999
Venules	Controls vs.Seizures+saline	New pericyte vs. Pre-exisiting pericyte	-0.7	1.69	>0.9999	6.5	2.68	0.2713
		Lost pericyte vs. No pericyte	-0.7	1.39	>0.9999	8.2	2.20	0.0074 **
	Controls vs.Seizures+PDGFbb	New pericyte vs. Pre-exisiting pericyte	-1.4	1.29	>0.9999	-10.9	2.05	<0.0001 ***
		Lost pericyte vs. No pericyte	1.0	1.20	>0.9999	-3.0	1.91	0.8238
	Seizures+saline vs.Seizures+PDGFbb	New pericyte vs. New pericyte+PDGFbb	-0.7	1.70	>0.9999	-17.4	2.70	<0.0001 ***
		Lost pericyte vs. Lost pericyte+PDGFbb	1.6	1.42	>0.9999	-11.2	2.26	<0.0001 ***

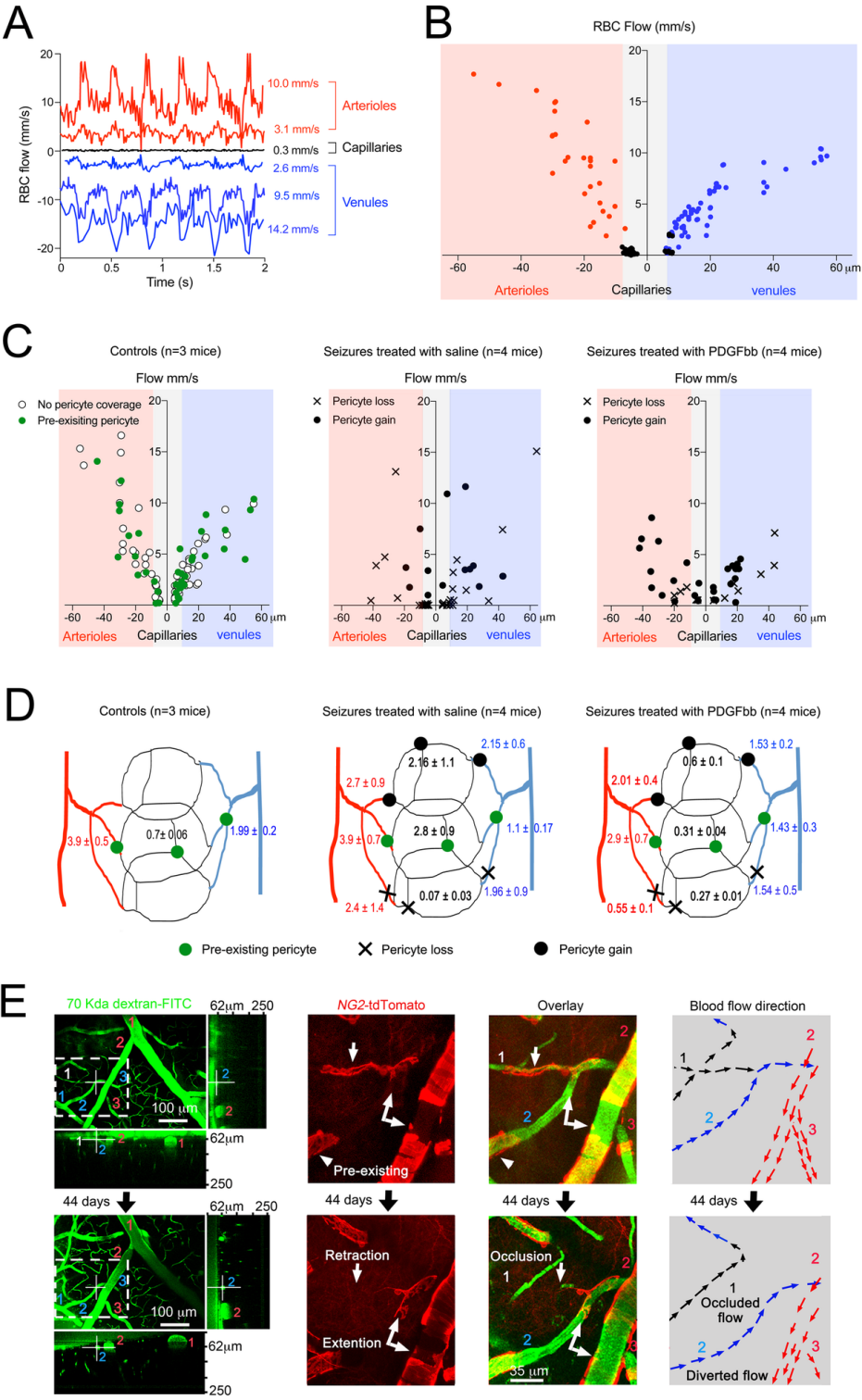
A
RBC flow (mm/s)
Time (s)
10.0 mm/s
3.1 mm/s
0.3 mm/s
2.6 mm/s
9.5 mm/s
14.2 mm/s
Arterioles
Capillaries
Venules
B
RBC Flow (mm/s)
Arterioles
Capillaries
venules
C
Controls (n=3 mice)
Seizures treated with saline (n=4 mice)
Seizures treated with PDGFbb (n=4 mice)
Flow mm/s
No pericyte coverage
Pre-exisiting pericyte
Pericyte loss
Pericyte gain
Arterioles
Capillaries
venules
D
Controls (n=3 mice)
Seizures treated with saline (n=4 mice)
Seizures treated with PDGFbb (n=4 mice)
3.9 ± 0.5
0.7± 0.06
1.99 ± 0.2
2.7 ± 0.9
2.16 ± 1.1
2.15 ± 0.6
3.9 ± 0.7
2.8 ± 0.9
1.1 ± 0.17
2.4 ± 1.4
0.07 ± 0.03
1.96 ± 0.9
2.01 ± 0.4
0.6 ± 0.1
1.53 ± 0.2
2.9 ± 0.7
0.31 ± 0.04
1.43 ± 0.3
0.55 ± 0.1
0.27 ± 0.01
1.54 ± 0.5
Pre-existing pericyte
Pericyte loss
Pericyte gain
E
70 Kda dextran-FITC
62µm
250
100 µm
44 days
NG2-tdTomato
Pre-existing
Retraction
Extention
Overlay
Occlusion
35 µm
Blood flow direction
Occluded flow
Diverted flow

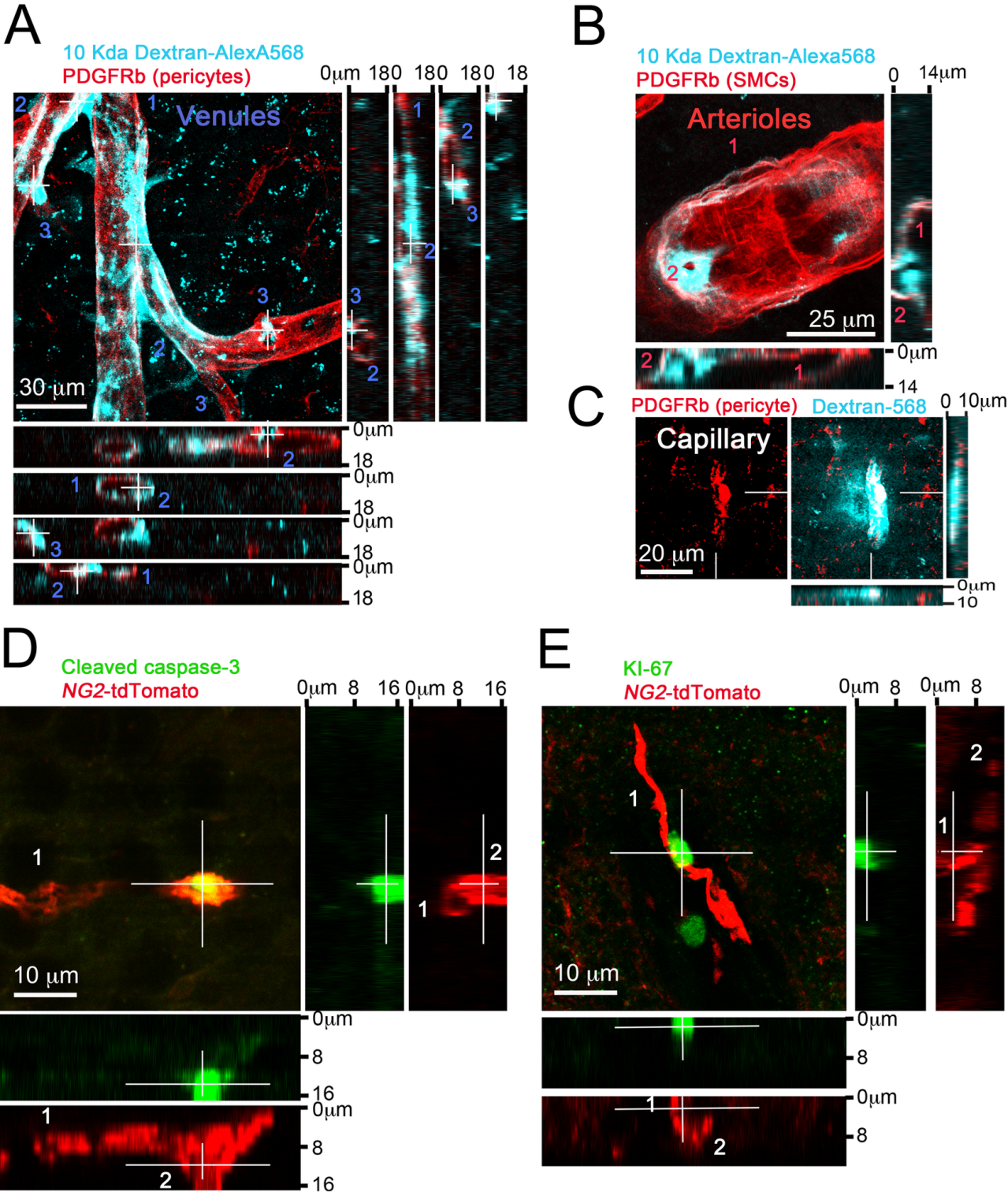
A
10 Kda Dextran-AlexA568
PDGFRb (pericytes)
Venules
30 μm
0μm 180 180 180 18
0μm
18
B
10 Kda Dextran-Alexa568
PDGFRb (SMCs)
Arterioles
25 μm
0 14μm
0μm
14
C
PDGFRb (pericyte)
Dextran-568
Capillary
20 μm
0 10μm
0μm
10
D
Cleaved caspase-3
NG2-tdTomato
10 μm
0μm 8 16 0μm 8 16
0μm
8
16
E
KI-67
NG2-tdTomato
10 μm
0μm 8 0μm 8
0μm
8